Steel and Composite Structures, *Vol. 33, No. 2 (2019) 225-243*
DOI: https://doi.org/10.12989/scs.2019.33.2.225

Effect of angle stiffeners on the flexural strength and stiffness of cold-formed steel beams

M. Adil Dar [1], N. Subramanian [2], Amer I. Rather [3], A.R. Dar*[3], James B.P. Lim [4], M. Anbarasu [5] and Krishanu Roy [4]

[1] *Department of Civil Engineering, Indian Institute of Technology Delhi, New Delhi, India*
[2] *Consulting Engineer, Maryland, USA*
[3] *Department of Civil Engineering, National Institute of Technology Srinagar, J&K, India*
[4] *Department of Civil & Environmental Engineering, University of Auckland, New Zealand*
[5] *Department of Civil Engineering, Government College of Engineering Salem, Tamil Nadu, India*

(*Received January 13, 2019, Revised August 23, 2019, Accepted October 1, 2019*)

Abstract. Cold-formed steel (CFS) sections when used as primary load carrying members often require additional strengthening for retrofitting purposes. In some cases, it is also necessary to reduce deflections in order to satisfy serviceability requirements. The introduction of angle sections, screwed to the webs so as to act as external stiffeners, has the potential to both increase flexural strength as well as reduce deflections. This paper presents the results of ten four-point bending tests, on built-up CFS sections, both open and closed, with different stiffening arrangements. In the laboratory tests, the stiffening arrangements increased the moment capacity and stiffness of the CFS beams by up to 85% and 100% respectively. The increase in moment capacity was more evident for the open sections, while that reduction in deflection was largest for the closed sections.

Keywords: cold-formed steel; experiment; stiffening arrangements; buckling; flexural strength

1. Introduction

In recent years, the use of cold formed steel (CFS) sections for the primary load bearing member of housing (as shown in Fig. 1) has become more popular, providing a more sustainable solution than other materials to the growing demand for low-cost houses (Khate *et al*. 2018, Kim *et al*. 2015, Biggs *et al*. 2015, Roy *et al*. 2018, 2019, Dar *et al*. 2015a, 2018a, b, c, 2019a, b, Kumar and Sahoo 2016, Hancock 2016, Valsa Ipe *et al*. 2013, Young 2005). Higher grades of steel combined with the rolling of intermediate stiffeners into the sections (as shown in Fig. 2) has resulted in CFS becoming an efficient building material (Wang and Young 2014, 2016, Haidarali and Nethercot 2012). A summary of the major developments on CFS members is given in Hancock (Hancock 2016). In terms of stiffeners, recent developments include the incorporation of stiffened web openings for ease of service integration (Uzzaman *et al*. 2017) as shown in Fig. 3.

The aforementioned stiffeners have all been rolled into the sections as part of the rolling process. There is also a need to strengthen existing cold-formed steel sections, for retrofitting purposes. In some cases, it is also necessary to reduce deflections in order to satisfy serviceability requirements.

This paper proposes the introduction of cold-formed steel angle sections, screwed to the webs through self-drilling screws, so as to act as external stiffeners, as shown in Fig. 4.

Fig. 1 Cold-formed steel framing for residential housing (http://www.bundesteel.com)

This type of stiffening method is commonly used in hot-rolled steel beams with openings or copes, where a steel plate acting as a stiffener is welded to the web of I-beam (Yam *et al*. 2007, 2011, Yang and Lui 2012). Providing horizontal stiffeners alone does not efficiently improve the web capacity in coped steel beams. Adequately designed vertical stiffeners, in combination with horizontal stiffeners, helps to achieve the improvement in the web buckling strength (Yam *et al*. 2007, 2011). The openings provided in the web for the utility purposes reduces its strength considerably (Lawson *et al*. 2006, Wanniarachchi *et al*. 2017, Keerthan and Mahendran 2013, Acharya *et al*. 2013). The number of openings and the size as well as the shape of the openings influences the flexural behavior of the CFS beams (Lawson *et al*. 2006, Wanniarachchi *et al*. 2017,

*Corresponding author, Professor,
E-mail: abdulrashid@nitsri.net

http://www.techno-press.org/?journal=scs&subpage=6

ISSN: 1229-9367 (Print), 1598-6233 (Online)

(a) CFS sections with intermediate stiffeners (Wang and Young 2014)

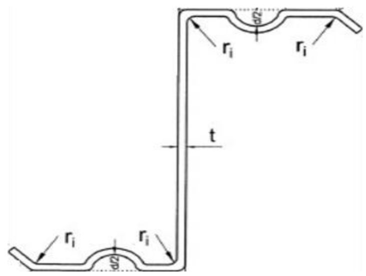

(b) Intermediate stiffening of flanges (Haidarali and Nethercot 2012)

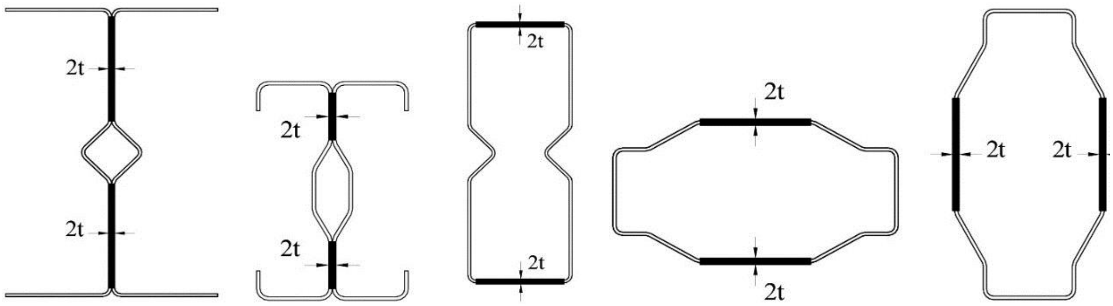

(b) Intermediate stiffening of webs (Wang and Young 2016)

Fig. 2 CFS sections with intermediate stiffeners

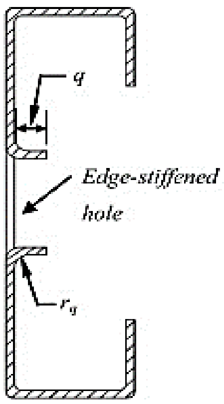

Fig. 3 CFS Section with edge-stiffened holes (Uzzaman *et al*. 2017)

Keerthan and Mahendran 2013, Acharya *et al*. 2013). In the past, different reinforcement measures like connecting a solid plate around the opening, connecting another joist section around the opening and bridged channel sections around the opening were adopted (Acharya *et al*. 2013) as shown in Fig. 5. However, the literature does not contain any strengthening of CFS sections with angle stiffening arrangements, as shown in Fig. 4. Apart from the type of intermittent stiffening of the webs as shown in Fig. 2, a cut made in the web of the channel section and, and then pulled out to serve as a vertical stiffener has also been studied (Šakalysa and Daniūnas 2017), as shown in Fig. 6. Furthermore, limited research work on external stiffening of CFS elements has been carried out, which includes options like the web strengthening of CFS beams using FRP laminates (Islam and Young 2013, 2014). As can be seen in Fig. 4, the CFS angle stiffeners back-to-back through the web of results in a simple installation process that can be used for existing CFS structures. Such stiffeners has the potential to both increase flexural strength as well as reduce deflections.

This paper presents the results of ten four-point bending tests, on both built-up open sections (formed by the two lipped channel sections were connected back-to-back using self-drilling screws spaced at 250 mm centre to centre longitudinally in two rows on the web, as shown in Fig. 7(a)) and closed CFS sections (the two lipped channel sections (with lip only in one direction) were joined toe-to-toe using self-drilling screws spaced 250 mm centre to centre in the longitudinal direction on the flange as shown in Fig. 7(b)), with different stiffening arrangements (vertical, longitudinal, diagonal and cross-diagonal stiffeners) as shown in Fig. 8.

2. Experimental investigation

2.1 Test specimens

Ten four point bending tests were conducted. Fig. 7 shows details of the cross-section of the CFS sections tested. The cross-sections of the specimens were designed such that the web was the weakest element of the cross-section, and was accordingly the only element that was stiffened. The compactness of the web (h/t = 156 > 70) was low. It was low enough to prevent local shear buckling. On the other hand, the compactness of the flange (b/t = 37.5 < 60) was substantially kept within the limits recommended

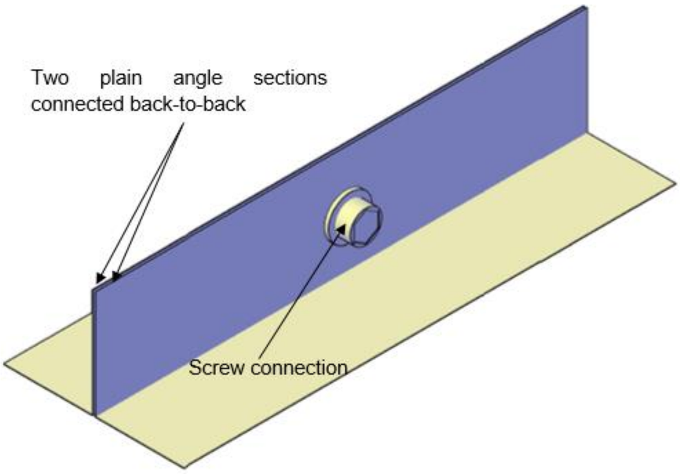

(a) Angle stiffener

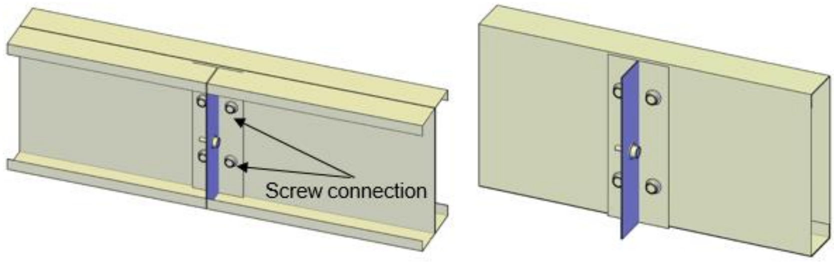

(b) Angle stiffener connected to the web of the channel sections in vertical direction.

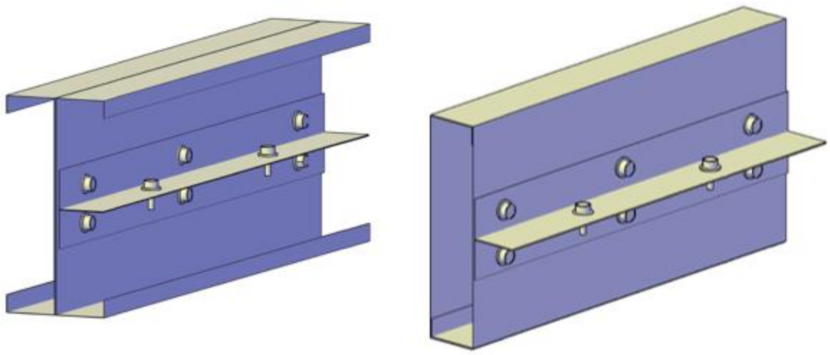

(c) Angle stiffener connected to the web of the channel sections in longitudinal direction.

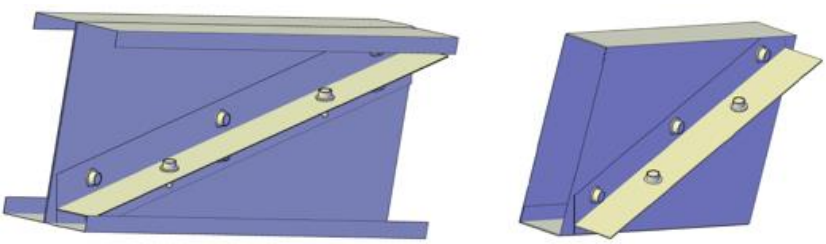

(d) Diagonal angle stiffener connected to the web of the channel sections

Fig. 4 Simplicity of novel stiffening arrangement in CFS beam sections

by different standards in order to control its buckling. Furthermore, a lip of considerable width was introduced to strengthen the flange against local buckling. This justifies the reason to stiffen the web alone.

The overall length of each specimen was 2.3 m, with a length of 2.1 m between supports. All sections were fabricated from locally available mild steel sheets of 1.6 .mm thickness. The tests comprised of:

(a) Five built up open sections (Fig. 8)
(b) Five built-up closed sections (Fig. 8)

For the open sections, the two lipped channel sections were connected back-to-back using self-drilling screws spaced at 250 mm centre to centre longitudinally in two rows on the web, as shown in Fig. 7(a). The rows were spaced at 83.33 mm along the depth of the section.

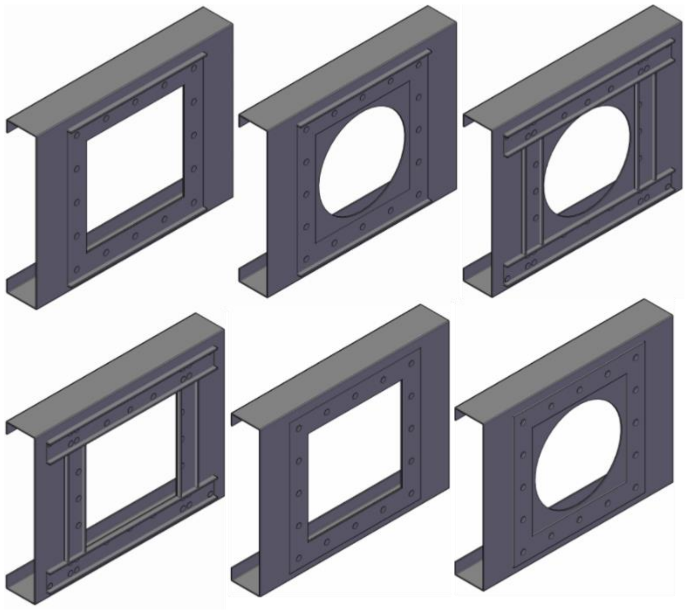

Fig. 5 Different reinforcement schemes adopted for CFS sections with web openings (Acharya *et al*. 2013)

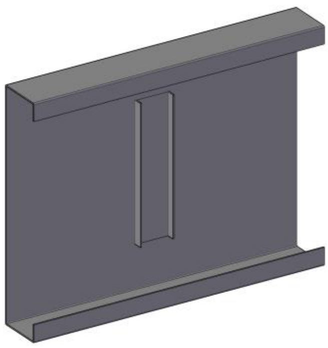

Fig. 6 Vertical stiffening of web (Sakalysa and Daniunas 2017)

For the closed sections, the two lipped channel sections (with lip only in one direction) were joined toe-to-toe using self-drilling screws spaced 250 mm centre to centre in the longitudinal direction on the flange as shown in Fig. 7(b). The stiffeners were CFS angle sections, from the same steel sheet, back-to-back as shown in Fig. 9.

2.2 Specimens labelling

The specimens were labelled such that the specimen's name represents its description in short form. For example, B-CDS represents Box beam with cross-diagonal stiffeners (B: box, C: cross, D: diagonal, S: stiffeners). The labelling details of various specimens are given in Table 1. Table 2 and Fig. 7 shows the nominal and measures dimensions of the test specimens. A Vernier caliper was used for measuring the dimensions of the different cross-sectional components of the test specimens.

2.3 Geometrical imperfections

The initial geometric imperfections of the specimens

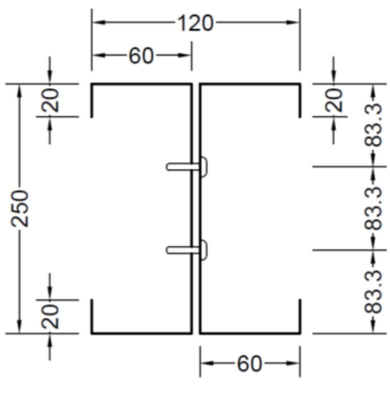

(a) Open section (I section)

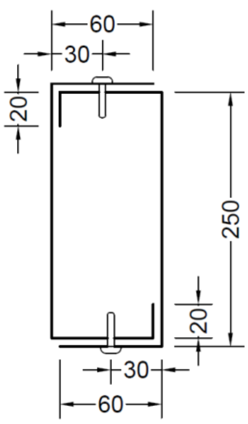

(b) Closed section (Box section)

Fig. 7 Cross-sectional profiles of the beams specimens

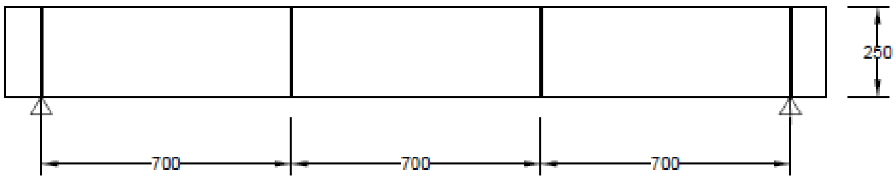

(a) Detailing of the stiffeners in elevation for control specimens (I-CB and B-CB)

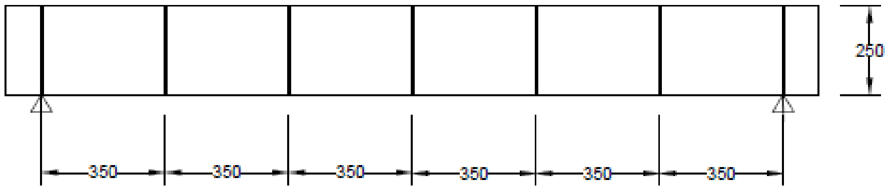

(b) Detailing of the stiffeners in elevation for specimens with vertical stiffeners (I-VS and B-VS)

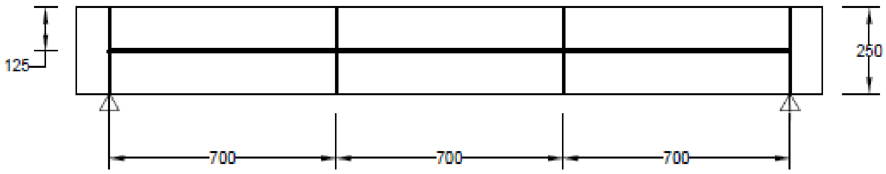

(c)Detailing of the stiffeners in elevation for specimens with longitudinal stiffeners (I-LS and B-LS)

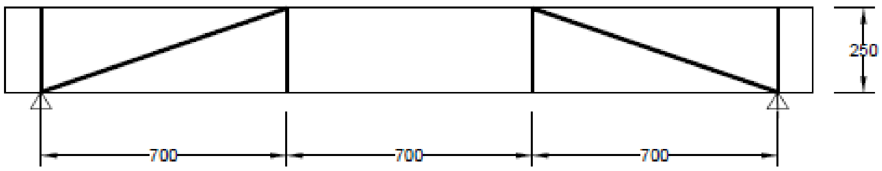

(d) Detailing of the stiffeners in elevation for specimens with diagonal end stiffeners (I-DS and B-DS)

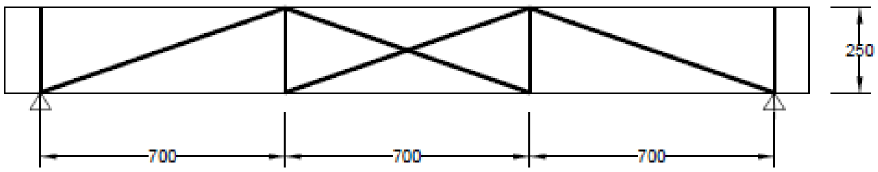

(e) Detailing of the stiffeners in elevation for specimens with cross-diagonal stiffeners (I-CDS and B-CDS)

Fig. 8 Detailing of the stiffeners in various specimens

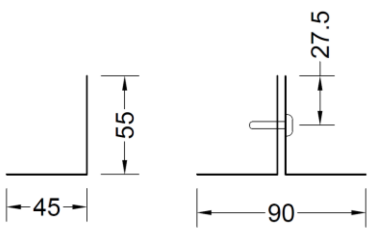

Fig. 9 Cross-sectional details of the stiffener used

were measured in two orthogonal directions (see Fig. 10). The imperfections were measured at the bottom flange to web junctions near the center. An optical theodolite and a calibrated digital Vernier caliper were used to obtain the readings at mid-span and near both ends of the test specimens. The imperfections measured at the mid-span along the specimen in the two orthogonal directions are given in Table 3. The maximum geometric imperfection measured at the mid-span in δ1 & δ2 direction was 1/3154 mm and 1/3052 mm, respectively, and were recorded in I-VS, while as the minimum imperfection was observed for B-CDS at the mid-span and were recorded as 1/4366, 1/3993 in δ1 & δ2 directions respectively. As a comparison, the magnitude of the maximum and minimum imperfections measured by (Fratamico *et al*. 2018) were 1/1092 and 1/7648, respectively.

2.4 Description of specimens

2.4.1 Control I Beam (I-CB)

I-CB acts as control (reference) model for other built-up pen specimens. It consists of basic I-profile geometry (fabricated by joining two lipped channel sections back-to-back). Load bearing stiffeners (fabricated by joining two angle sections back-to-back as discussed previously) are provided at two loading and reaction points in order to prevent the crippling effects in the web due to concentrated

Table 1 Labelling description of various specimens

Specimen label	Specimen description
I-CB	Control I Beam
I-VS	I beam with Vertical Stiffeners
I-LS	I beam with Longitudinal Stiffeners
I-DS	I beam with Diagonal end Stiffeners
I-CDS	I beam with Cross-Diagonal Stiffeners
B-CB	Control Box Beam
B-VS	Box beam with Vertical Stiffeners
B-LS	Box beam with Longitudinal Stiffeners
B-DS	Box beam with Diagonal end Stiffeners
B-CDS	Box beam with Cross-Diagonal Stiffeners

loading. Details of I-CB are shown in Fig. 8(a).

2.4.2 I beam with vertical stiffeners (I-VS)

In addition to I-CB, I-VS consists of three more pairs of vertical stiffeners, each between the load bearing stiffeners (on each side of specimen) as shown in Fig. 8(b). The spacing between vertical stiffeners is kept at 350 mm centre to centre of the stiffener along the span of the beam specimen. The configuration of stiffening arrangement was adopted on the basis that the elastic buckling stress (fcr) of a thin flat plate of length L, depth d, and thickness t, simply supported along all four edges and loaded by shear stresses distributed uniformly along its edges may be significantly increased by using intermediate vertical stiffeners, which will decrease the aspect ratio L/d, thus increasing the value

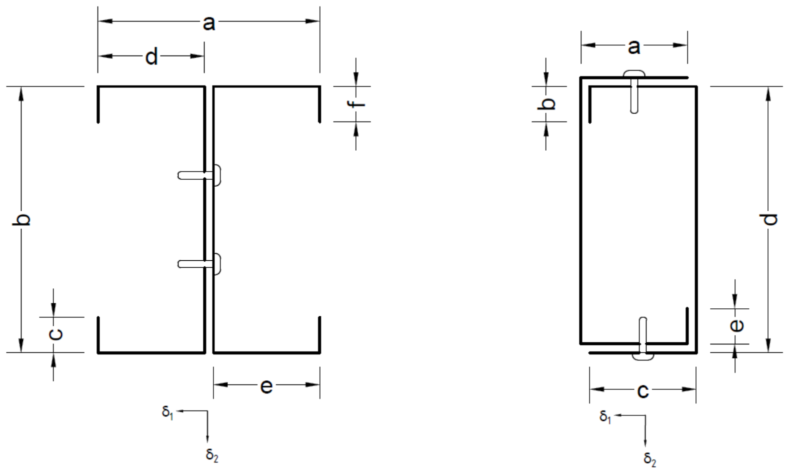

Fig. 10 Dimensional details and directions of geometric imperfection measurement.

Table 2 Dimensional details of the specimens

Specimen	Weight (kg)	Nominal (mm)						Measured (mm)					
		a	b	c	d	e	f	a	b	c	d	e	f
I-C	26.64	120	250	60	60	20	20	121	253	60	60	19	18
I-VS	30.14	120	250	60	60	20	20	121	251	60	61	18	19
I-LS	35.82	120	250	60	60	20	20	122	251	59	61	18	19
I-DS	34.16	120	250	60	60	20	20	122	251	61	59	19	19
I-CDS	41.68	120	250	60	60	20	20	123	248	59	62	21	20
B-C	25.58	60	250	60	20	20	-	60	249	61	20	19	-
B-VS	29.35	60	250	60	20	20	-	60	252	59	20	20	-
B-LS	34.76	60	250	60	20	20	-	58	254	59	21	20	-
B-DS	33.1	60	250	60	20	20	-	61	250	60	21	19	-
B-CDS	40.62	60	250	60	20	20	-	61	248	62	17	18	-

Table 3 Geometric imperfections measured in the specimens

Specimen	I-CB	B-CB	I-VS	B-VS	I-LS	B-LS	I-DS	B-DS	I-CDS	B-CDS
δ1/L	1/3443	1/3625	1/3154	1/3432	1/3847	1/4203	1/3526	1/4183	1/4225	1/4366
δ2/L	1/3763	1/3332	1/3052	1/3282	1/3526	1/3873	1/3681	1/3823	1/3708	1/3993

of the buckling coefficient k. The increase in k value further leads to increase in elastic buckling stress. Hence, such a plate element will carry higher loading. Further, the addition of vertical stiffeners reduces the half-wave local buckling along the span of the beams in the web region, which may improve the capacity of these beams. These stiffeners also may improve the elastic buckling strength of the flanges.

$$f_{cr} = \frac{\pi^2 E}{12\,(1-\mu^2)} \frac{k}{(d/t)^2} \qquad (1)$$

where, μ is Poisson's ratio of the material, d/t is the plate slenderness, E is the young's modulus of the material and k is the buckling coefficient and is approximated by

$k = 5.35 + 4(d/L)^2$ when $L \geq d$, and
$k = 5.35(d/L)^2 + 4$ when $L \leq d$.

2.4.3 I beam with longitudinal stiffeners (I-LS)

In addition to I-CB, I-LS consists of three more pairs of longitudinal stiffeners (on each side of sample) between the top flanges and the bottom flanges of the channel sections comprising the built-up section as shown in Fig. 8(c). The longitudinal stiffeners were provided between the bearing stiffeners along central longitudinal axis of the beam. The selection of such a configuration was made on the basis that adoption of longitudinal stiffeners leads to the drop in the depth-thickness (d/t) ratio, which increased the elastic critical buckling stress. Hence, such a plate element will carry higher loading. Furthermore, the incorporation of longitudinal stiffeners reduces the half-wave local buckling along the depth of the beams in the web region, which may improve the capacity of these beams. These stiffeners also improved the elastic buckling strength of the flanges by further stiffening of the bearing stiffeners. Overall, the chances of web induced buckling will drop in these beams.

2.4.4 I beam with diagonal end stiffeners (I-DS)

In addition to I-CB, I-DS consists of two more pairs of diagonal stiffeners (on each side of the specimen) between the load bearing stiffeners in the shear zone as shown in Fig. 8(d). In order to safeguard the web effectively against both shearing and bending buckling stresses, combination of vertical, diagonal stiffeners should be used (Subramanian 2016). Moreover, by placing the stiffeners diagonally across each panel, a truss like action is rendered by the stiffeners, thereby carrying a portion of the load in addition to preventing buckling (Azmi *et al*. 2017). These were the primary causes of adopting such a stiffening configuration. Furthermore, the chances of web induced buckling will drop in these beams.

2.4.5 I beam with cross-diagonal stiffeners (I-CDS)

In addition to I-DS, I-CDS consists of a pair of cross-diagonal stiffeners placed in the pure moment zone as shown in Fig. 8(e). During the testing of IBDS and BBDS specimen, no buckling was observed in the shear zones (where diagonal stiffeners were adopted). However, major signs of buckling and distortion were observed in the central zones of these specimens. To prevent buckling in the central zone, a cross diagonal stiffener was adopted there. This justifies the selection of such a configuration of stiffening in this specimen. Furthermore, this configuration will enhance the alternative load path (truss action) as suggested by (Azmi *et al*. 2017). Also, the chances of web induced buckling will drop in these beams.

Specimens 6-10 consists of CFS built-up closed sections with the same stiffening arrangement as shown in Fig. against their corresponding CFS built-up open sections. Closed sections were adopted due to their inherent resistant against torsional buckling. In order to evaluate the performance of these novel stiffening arrangements in CFS built-up closed sections, such sections were adopted.

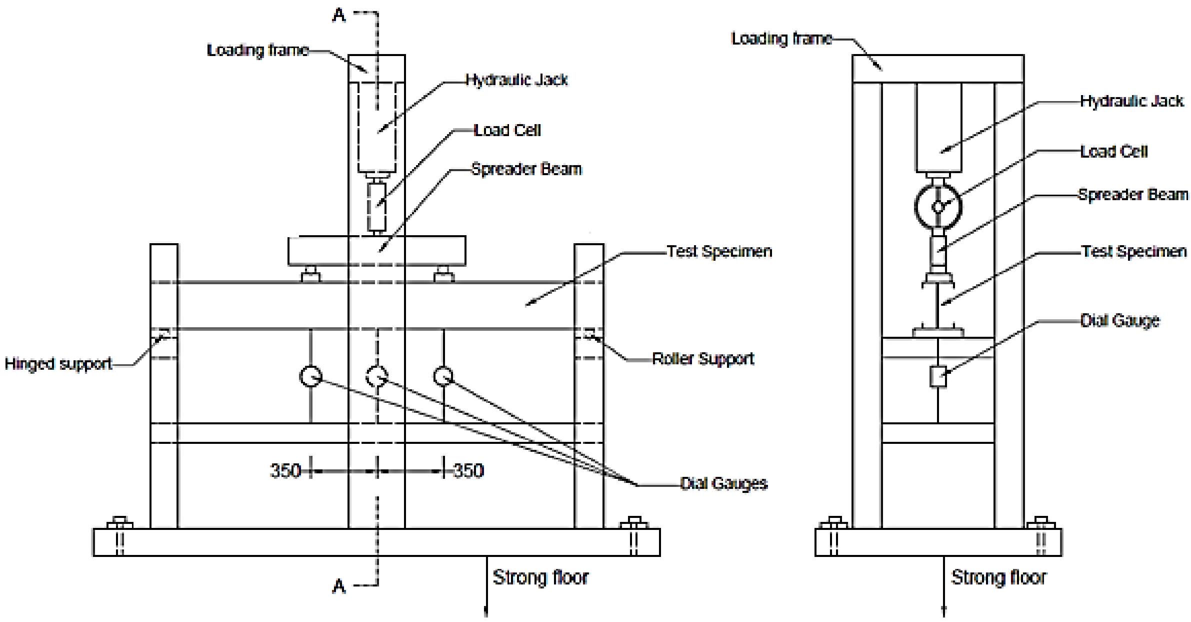

Fig. 11 Schematic view of the testing arrangement

Table 4 Material properties of steel used

S. No	f_y (MPa)	f_u (MPa)
Coupon-1	372.30	422.37
Coupon-2	361.16	414.75
Coupon-3	377.08	417.93
Coupon-4	369.01	447.74
Coupon-5	360.21	425.37

2.5 Material properties

Mild steel sheets of size 1250 mm × 2500 mm × 1.6 mm conforming to the Indian Standard (IS 2062-2011) were used for the fabrication of the specimens. The steel sheets belong to grade E250 with quality designation 'A'. For the determination of the mechanical properties of the material used, the Indian Standard (IS 1608-2005) prescribes the procedure for conducting a tensile test on a steel strip (0.5 mm < thickness 3 mm). The same procedure was adopted for the testing of the coupons. A universal testing machine was used to conduct the tensile testing of five coupons that were prepared from the web plate of the untested specimens in the longitudinal direction. A displacement controlled computerized universal testing machine with friction grips was used for the testing of coupons. The various material properties obtained from the tests are given in Table 4. The mean value of 363.95 N/mm^2 for yield strength (f_y), 425.64 N/mm^2 for ultimate strength (f_u) and 201 GPa for Modulus of Elasticity (E) was obtained.

3. Test results

During the testing of the various specimens, it was observed that initially small local buckling was initiated in the lip for open sections and in the flange for closed sections predominantly in the moment zone. However, the magnitude of this local buckling instability was very small. The major signs of local buckling were observed in the web (in the moment zone) of the specimens, which intensified during the final stages of loading. In addition to this, the compression flanges under the concentrated loading points also suffered from large local buckling failures towards the end of the loading, mainly due to the web stiffening at those locations.

Fig. 12 shows the load *vs.* mid-span displacement plots for open and closed CFS beam specimens. The load *vs.* mid-span displacement response of the I-CB specimen was nearly linear up to a load of 29.41 kN as shown in Fig. 12(a). A smooth increasing trend of the curve confirms the beam action of the specimen. At a load of 29.41 kN, the specimen began to show signs of lateral torsional buckling. After this load, the rate of deformation increased up to a load of 37.37 kN, and the lateral torsional buckling in the specimen became more evident. This can be depicted from the kink observed in the load *vs.* mid-span displacement response of this specimen. Beyond this point, the specimen did not carry any further loading, instead a drop in the load *vs.* mid-span displacement curve was observed. Small buckling of the load bearing stiffeners was also observed. This specimen carried a maximum load of 37.37 kN with a corresponding mid-span displacement of 6.19 mm. Lateral torsional buckling accompanied by local buckling was the mode of failure observed, as shown in Fig. 13.

The load *vs.* mid-span displacement of the I-VS specimen behaved linearly up to a load of 60.05 kN as shown in Fig. 12(a). Early sign of minor buckling in the lip of the compression flange near one of the loading points (in the moment zone) was observed at a load of about 30.02 kN. As the loading increased, this lip buckling also increased, and finally it was visibly evident at a load of about 44.73 kN as shown in Fig. 14(a). Further, the web of the specimen started to buckle inwards at some locations and outwards at the other locations (in the moment zone of the specimen) which increased towards failure load as shown in Fig. 14(b). Beyond this point, the specimen did not carry any further loading, instead a drop in the load *vs.* mid-span displacement curve was observed. No signs of torsion were observed in this case. The specimen carried a maximum load of 60.05 kN with a corresponding mid-span displacement of 7.94 mm. Local buckling in flange and

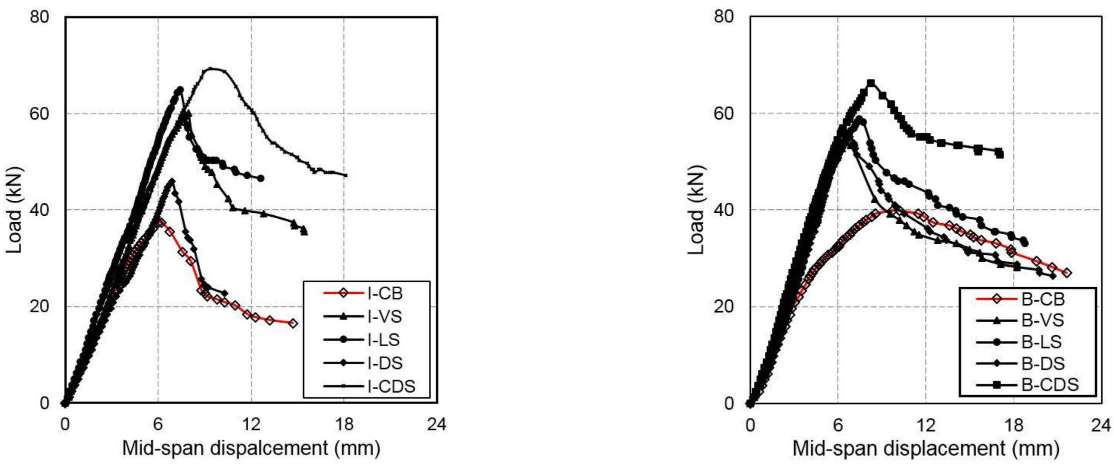

(a) Open CFS beam specimens (b) Closed CFS beam specimens

Fig. 12 Load *vs.* mid-span displacement plots for open and closed CFS beam specimens

Fig. 13 Failure in I-CB specimen

central web portion were the modes of failure observed as shown in Fig. 14.

The load *vs.* mid-span displacement of the I-LS specimen behaved linearly up to a load of 64.95 kN as shown in Fig. 12(a). The smooth curve confirms the beam action of the model. Local buckling in the lip of the compression flange near one of the loading points (in the moment zone) was observed at a load of about 32.47 kN, which increased towards failure load (64.95 kN) as shown in Fig. 15(a). Beyond this point, the specimen did not carry any further loading, instead a drop in the load *vs.* mid-span displacement curve was observed. No signs of torsion were observed in this case as well. However, lateral buckling along the minor axis was observed after unloading as shown in Fig. 15(b). This specimen carried a maximum load of 64.95 kN with a corresponding mid-span displacement of 7.44 mm. Local buckling in the lip of the compression flange and lateral buckling along the minor axis were the modes of failure observed as shown in Fig. 15.

The load *vs.* mid-span displacement of the I-DS specimen behaved linearly up to a load of 45.96 kN as shown in Fig. 12(a). At a load of 25.12 kN, the specimen began to show signs of lateral torsional buckling, which dominated towards the failure load (45.96 kN) as shown in Fig. 16. This can be depicted from the kink observed in the load *vs.* mid-span displacement response of this specimen. Beyond this point, the specimen did not carry any further loading, instead a drop in the load *vs.* mid-span displacement curve was observed. This specimen carried a maximum load of 45.95 kN with a corresponding mid-span displacement of 6.75 mm. Lateral torsional buckling in the specimen was the mode of failure observed.

(a) Lip buckling of the compression flange at a load of 44.73 kN

(b) Web buckling in the specimen

Fig. 14 Failure in I-VS specimen

(a) Local buckling in the lip of the compression flange

(b) Lateral buckling along minor axis

Fig. 15 Failure in I-LS specimen

The load *vs.* mid-span displacement of the I-CDS specimen behaved linearly up to a load of 69.24 kN as shown in Fig. 2(a). Early sign of minor buckling in the lip of the compression flange as well as the compression flange near one of the loading points (in the moment zone) was observed at a load of about 35.53 kN was observed and this behavior increased until failure load (69.24 kN) as shown in Fig. 17(a). Beyond this point, the specimen did not carry any further loading, instead a drop in the load *vs.* mid-span displacement curve was observed. The drop of the load was gradual compared to other models. Lateral buckling along the minor axis was also observed after unloading as shown in Fig. 17(b). This specimen carried a maximum load of 69.24 kN with a corresponding mid-span displacement of 9.38 mm. Local buckling in the compression flange including its lip and lateral buckling along the minor axis were the modes of failure observed as shown in Fig. 17.

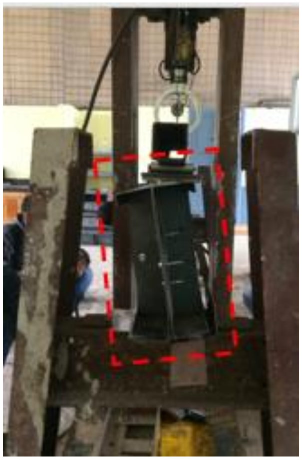

Fig. 16 Lateral torsional buckling in the I-DS specimen

The load *vs.* mid-span displacement of the B-CB specimen behaved almost linearly up to a load of 28.79 kN as shown in Fig. 12(b). Beyond this point, a slight curvature in the curve is observed up to a load of 39.82 kN. Local buckling in compression zone of the central portion started at a load of 28.79 kN as shown in Fig. 18(a). Towards the failure load (39.82 kN), web buckling started around the

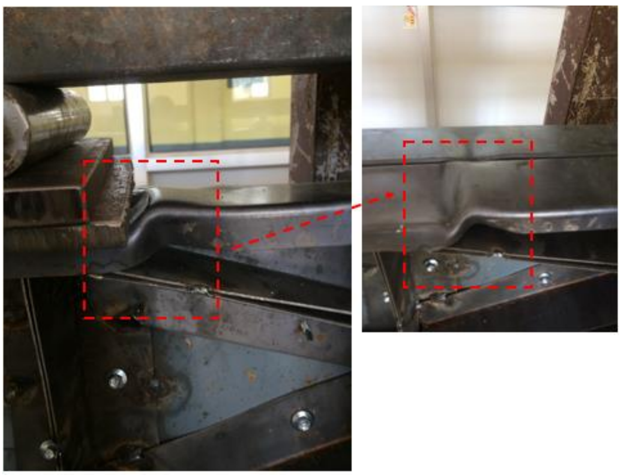

(a) Local buckling in the compression flange portion

(b) Lateral buckling along minor axis

Fig. 17 Failure in I-CDS specimen

(a) Local buckling in the compression flange

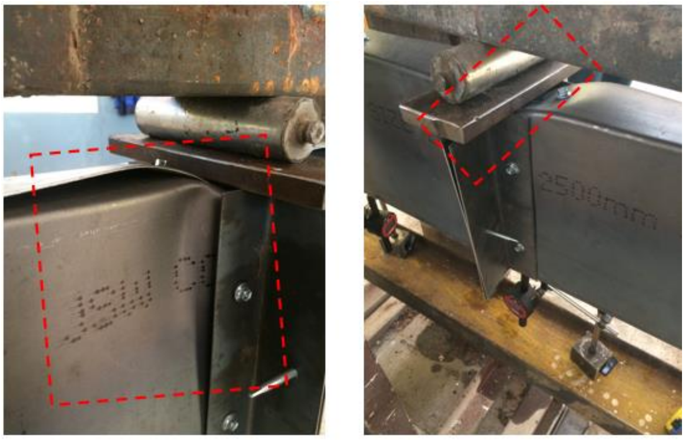

(b) Web and flange buckling due to crushing effect of concentrated load

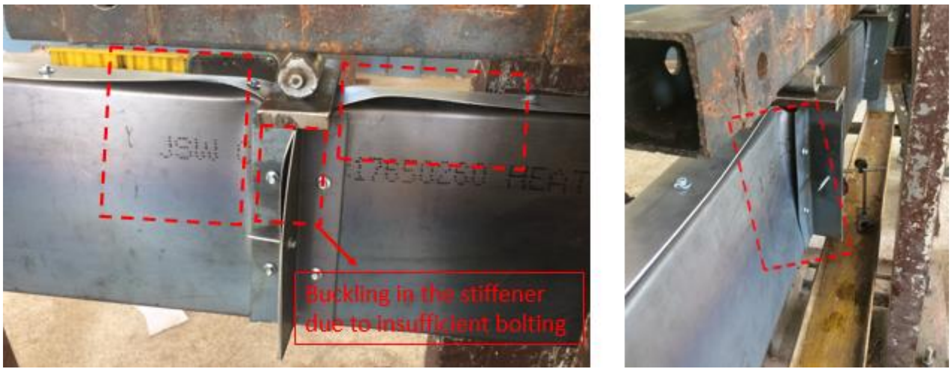

(c) Bearing failure under the loading point

Fig. 18 Failure in B-CB specimen

loading region and the flanges also started experiencing local buckling, primarily due to the web crippling effect of concentrated loading as shown in Fig. 18(b). This finally led to bearing failure at that loading point as shown in Fig. 18(c). Beyond this point, the specimen did not carry any further loading, instead a drop in the load vs. mid-span displacement curve was observed. No signs of torsion were observed in this case. The specimen carried a maximum load of 39.82 kN with a corresponding mid-span displacement of 9.70 mm. Local buckling in compression flange and web under the loading point were the modes of failure observed as shown in Fig. 18.

The load *vs*. mid-span displacement of the B-VS specimen behaved almost linearly up to a load of 50.85 kN. Early sign of minor local buckling in the compression flange was observed at a load of about 34.31 kN. Before failure load of 53.31kN was reached, web buckling between loading points (0.85 m from the left support) was observed as shown in Fig. 19, and can be depicted from the minor curvature in the upper part of the rising curve. Beyond this point, the specimen did not carry any further loading, instead a drop in the load vs. mid-span displacement curve was observed. No signs of torsion were observed in this case. This specimen carried a maximum load of 53.31 kN with a corresponding mid-span displacement of 6.86 mm. Local buckling in compression flange and web near the loading point (in the moment zone) were the modes of failure observed as shown in Fig. 19.

The load *vs*. mid-span displacement of the B-LS specimen behaved nearly linear up to a load of 48 kN. Minor local buckling in the compression flange (in the moment zone) was observed at a load of about 34.31 kN, which kept on increasing towards the failure load (58.21 kN) as shown in Fig. 20(a). Web buckling in the form of a half wave like pattern was observed moment zone (some portion moving inwards, some outwards) at a load of

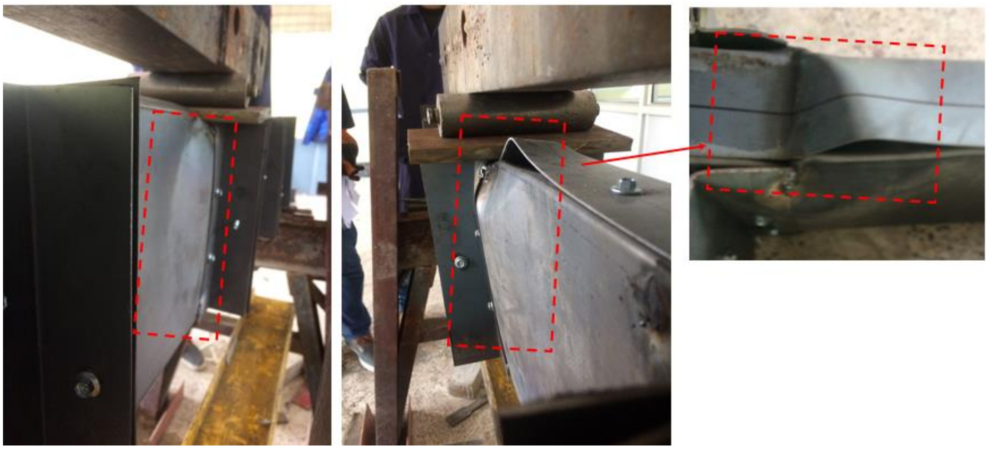

Fig. 19 Web and flange buckling in B-VS

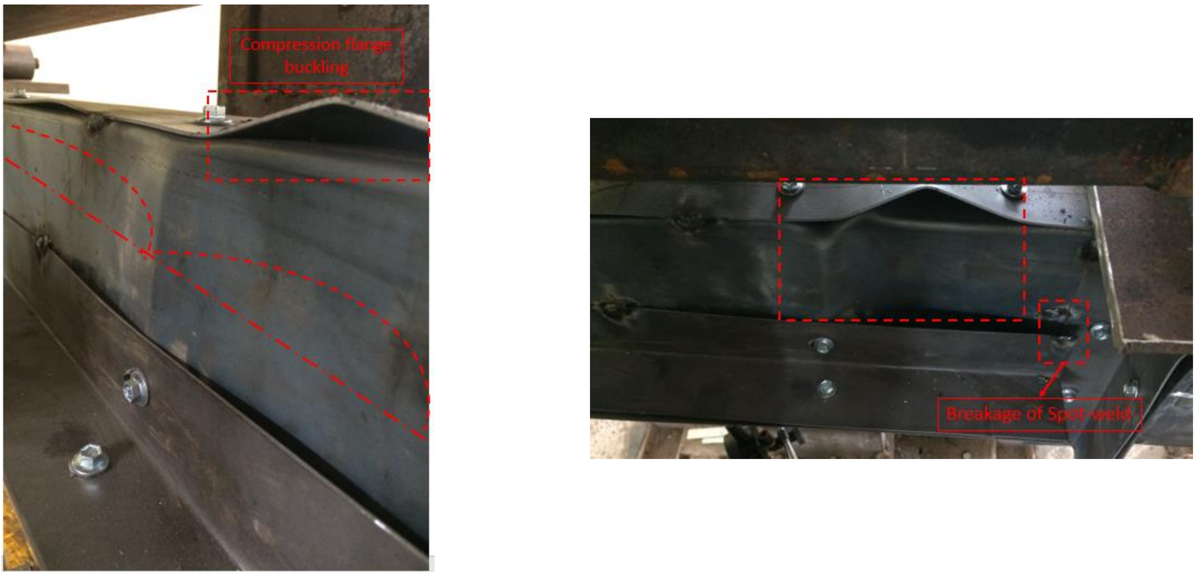

(a) Half waved web buckling and compression flange buckling

(b) Spot-weld breakage and increase in the amplitude of half- waved web buckling

Fig. 20 Failure in B-LS specimen

around 52.08 kN as shown in Fig. 20(a). In addition to this, the spot weld joining the longitudinal stiffener with the bearing stiffener broke, leading to small drop in the flexural stiffness and can be depicted by the minor kink observed at the load of 48 kN in the rising curve. This further increased the amplitude of the half wave web buckling until the failure load (58.21 kN) as shown in Fig. 20(b). Beyond this point, the specimen did not carry any further loading, instead a drop in the load vs. mid-span displacement curve was observed. No signs of torsion were observed in this case. This specimen carried a maximum load of 58.21 kN with a corresponding mid-span displacement of 7.7 mm. Local buckling in compression flange (in the moment zone) and half waved web buckling in the moment zone were the modes of failure observed as shown in Fig. 20.

The load *vs.* mid-span displacement of the B-DS specimen behaved nearly linear up to a load of 55.15 kN. The initiation of local buckling in the compression flange (in the moment zone) was observed at a load of about 36.76 kN as shown in Fig. 21(a), which kept on increasing towards the failure load (55.15 kN). The initiation of local web in the central zone of the specimen was observed at a load of around 42.89 kN. This effect was more pronounced near the loading points and continued to increase towards the failure load as shown in Fig. 21(b). Beyond this point, the specimen did not carry any further loading, instead a drop in the load vs. mid-span displacement curve was observed. No signs of torsion were observed in this case. This specimen carried a maximum load of 55.15 kN with a corresponding mid-span displacement of 6.75 mm. Local buckling in compression flange and web buckling in the moment zone were the modes of failure observed as shown in Fig. 21.

The load *vs.* mid-span displacement of the B-CDS specimen behaved nearly linear up to a load of 66.17 kN. Minor local buckling in the compression flange was observed in the moment zone of the specimen at a loading of 36.76 kN as shown in Fig. 22. Web buckling near the

(a) Initiation of local flange buckling at a load of 36.76 kN

(b) Web and compression flange buckling at failure load

Fig. 21 Failure in B-DS specimen

Fig. 22 Minor flange buckling in B-CDS specimen

centre of the specimen started to buckle at a load of around 53.30 kN which increased with the increase in the loading until the peak load of 66.17 kN. Beyond this, the model did not take any load, instead the model began to drop load slowly but the defection continued to increase. The drop of the load was gradual compared to other models. This specimen carried a maximum load of 66.17 kN with a corresponding mid-span displacement of 8.25 mm. Pure flexure failure (accompanied with minor local flange buckling) was the mode of failure observed. Fig. 23 shows the deformed shapes of all the tested specimens.

4. Design rules

The design strengths (moment capacities) of the open and closed CFS built-up sections were calculated using NAS (AISI S-100-2016) and IS (IS 801-2010). The CFS cross-sections excluding the novel stiffening arrangements were adopted for the design strength determination. It should be noted that the Load and Resistance Factor Design (LRFD) approach was adopted for determining the design strengths using the NAS (AISI S-100-2016), while as the Working Stress Method (WSM) was used for the same in

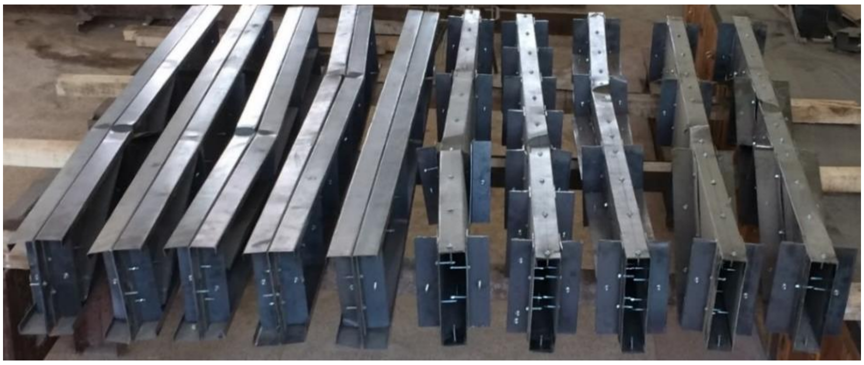

Fig. 23 Deformed shapes of the tested specimens

the IS (IS 801-2010) case. The design procedure of flexural members for both these standards are given below. The design strengths of both the series are presented in Table 5. Since the load transmitted by the loading jack on to the spreader beam was a point load, and was recorded as P_{Test}, for the sake of comparison the design moment capacities of both NAS (AISI S-100-2016) and IS (IS 801-2010) were used for determining the equivalent single point design load carrying capacities of these specimens, which are referred as P_{NAS} and P_{IS}.

4.1 Design rules specified in AISI-S100-16 (AISI S-100-2016)

4.1.1 Design strength

The unfactored design strength (M_n) of flexural members using the AISI specification is calculated as follows

$$M_n = S_e \times F_y \tag{2}$$

$$S_e = I_x / y_{cg} \tag{3}$$

Where F_y is the nominal yield strength, S_e is the elastic section modulus relative to top fibre, y_{cg} is the depth of neutral axis with respect to the compression flange and I_x is second moment of area of the effective section, determined by using a reduction factor, given by

$$b = w \qquad for \quad \lambda \leq 0.673 \tag{4}$$

or

$$b = \rho w \qquad for \quad \lambda > 0.673 \tag{5}$$

$$\lambda = \frac{1.052}{\sqrt{k}} \left(\frac{w}{t}\right) \frac{\sqrt{f}}{\sqrt{E}} \tag{6}$$

$$\rho = \frac{1 - 0.22/\lambda}{\lambda} \leq 1 \tag{7}$$

Where b = effective design width; w = width of compression element; ρ = reduction factor; k = plate buckling co-efficient; t = thickness of compression element; E = modulus of elasticity; f = maximum compressive edge stress in the element.

Table 5 Comparison of test results

(a) I sections

Specimen	P_{NAS} (kN)	P_{IS} (kN)	P_{Test} (kN)	M_{Test} (kNm)	M_y (kNm)	Z_{xc} 10^4 mm^3	Se 10^4 mm^3	M_p (kNm)	M_{Test}/M_y	M_{Test}/M_p	Failure modes
I-CB			37.37	13.08					0.55	0.46	LTB
I-VS			60.05	21.02					0.88	0.75	FB + WB
I-LS	45.51	40.66	64.95	22.73	23.72	9.84	8.81	28.08	0.96	0.81	LB + Lt.B
I-DS			45.96	16.09					0.68	0.57	LTB
I-CDS			69.24	24.23					1.02	0.86	FB + LB + Lt.B

(b) Box sections

Specimen	P_{NAS} (kN)	P_{IS} (kN)	P_{Test} (kN)	M_{Test} (kNm)	M_y (kNm)	Z_{xc} 10^4 mm^3	Se 10^4 mm^3	M_p (kNm)	M_{Test}/M_y	M_{Test}/M_p	Failure modes
B-CB			39.82	13.94					0.63	0.53	FB + WB
B-VS			53.31	18.66					0.84	0.71	FB + WB
B-LS	44.37	37.80	58.21	20.37	22.05	6.21	5.80	26.23	0.92	0.77	FB + WB
B-DS			55.15	19.30					0.87	0.73	FB + WB
B-CDS			66.17	23.16					1.05	0.88	Flxr.B

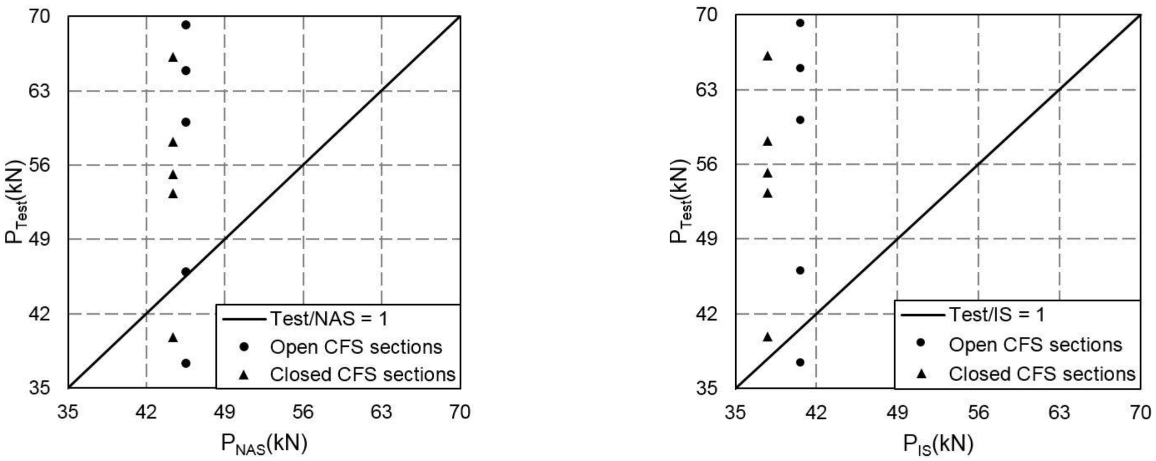

Fig. 24 Comparison of test results with the design strengths predictions

4.1.2 Lateral torsional buckling strength

The lateral torsional strength (M_n) of flexural members using the AISI specification is calculated as follows

$$M_n = F_c \times S_c \tag{8}$$

Where, S_c = elastic section modulus of effective section calculated related to extreme compression fibre at Fc.

For I-sections:

F_c will be determined as follows

For $F_e \geq 2.78\ F_y$, member is not subjected to lateral torsional buckling.

For $2.78\ F_y > F_e > 0.56\ F_y$

$$F_c = \frac{10}{9} F_y \left(1 - \frac{10F_y}{36F_e}\right) \tag{9}$$

For $F_e < 0.56\ F_y$

$$F_c = F_e \tag{10a}$$

Where F_y is yield strength and F_e is elastic lateral torsional buckling stress.

For Box sections:

$$F_e = \frac{C_b \pi}{K_y L_y S_f} \sqrt{EGJI_y} \tag{10b}$$

Where, J = torsional constant of the box, I_y = moment of inertia of the full unreduced section about centroidal axis parallel to web, G = shear modulus, E = modulus of elasticity, K_y = effective length factor for bending about y-axis, L_y = unbraced length of member for bending about y-axis, S_f = elastic section modulus of full unreduced section calculated related to extreme compression.

4.2 Design rules specified in IS-801 (IS 801-2010)

The code is based on working stress method and specifies the strength of flexural members as minimum obtained on the basis of yielding and lateral torsional buckling of the section.

4.2.1 Based on yielding

Nominal Moment

$$M = 0.6 \times f_y \times Z_{xc} \tag{11}$$

Where, F_y = Specified minimum yield point, Z_{xc} = Elastic section modulus of effective section.

4.2.2 Based on lateral torsional buckling

To avoid lateral buckling in the laterally unsupported beams, the peak compression stress on their extreme fibres should neither exceed the allowable stress (0.6 f_y) nor the following peak stresses when bending about the centroidal axis perpendicular to the web

Nominal Moment

$$M = f_b \times Z_{xc} \tag{12}$$

$$f_b = \frac{2}{3} f_y - \frac{{f_y}^2}{5.4\pi^2 E C_b} \left(\frac{L^2\ Z_{xc}}{d\ I_{yc}}\right) \tag{13}$$

when

$$\frac{0.36\pi^2 E C_b}{F_y} < \frac{L^2 Z_{xc}}{dI_{yc}} < \frac{1.8\pi^2 E C_b}{F_y} \tag{14}$$

$$f_b = 0.6\ \pi^2\ E C_b\ \left(\frac{d\ I_{yc}}{L^2\ Z_{xc}}\right) \tag{15}$$

When

$$\frac{L^2\ Z_{xc}}{dI_{yc}} \geq \frac{1.8\ \pi^2\ E\ C_b}{F_y} \tag{16}$$

L = unbraced length of the member, I_{yc} = the moment of inertia of the compression portion of the section about the gravity axis of the entire section parallel to the web, Z_{xc} = Compression section modulus of entire section about major axis, I_{xx} divided by distance to the extreme compression fiber, d = depth of the section, C_b = bending coefficient which can be conservatively taken as unity. Further details about this design procedure can be found elsewhere (SP 6 (5) - 1980).

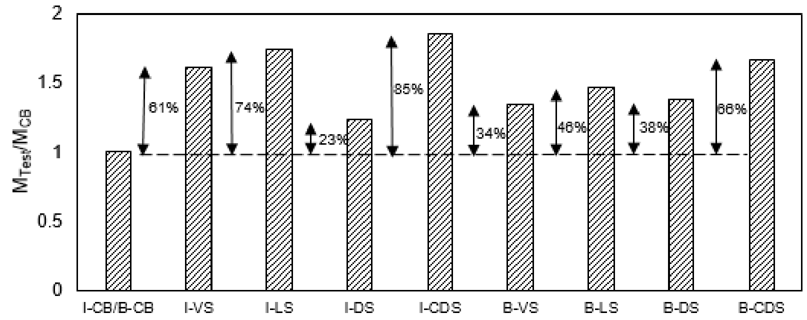

(a) Comparison of the flexural capacity

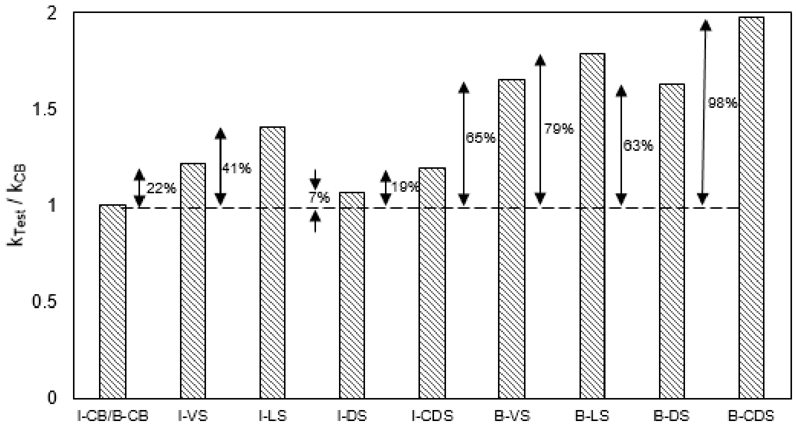

(b) Comparison of the stiffness characteristics

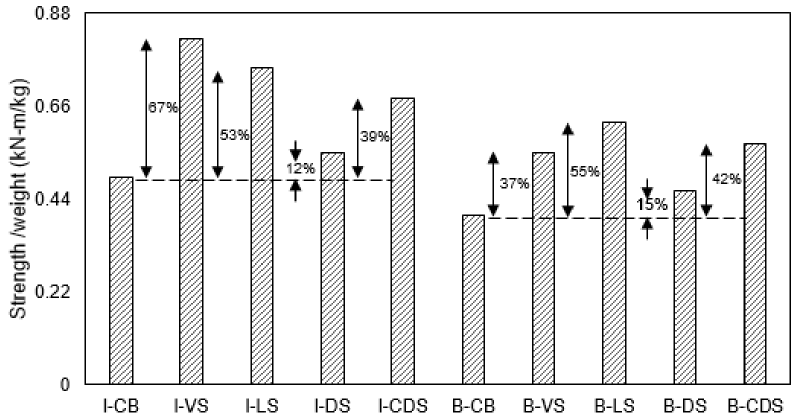

(c) Strength/weight comparison

Fig. 25 Efficiency comparison of open and closed series specimens

4.3 Comparison of test results

Table 5 and Fig. 24 shows the comparison of test results with the design strengths predicted by NAS (AISI S-100-2016) and IS (IS 801-2010). The test strength (P_{Test}) for each specimen given in Table 5 is the total load (being delivered by the loading jack) resisted by it. Based on the yield moment attaining capability and the possibility of plastic hinge development, steel sections are generally classified as plastic, compact, semi-compact and slender sections, which largely govern their behaviour, particularly the local buckling resistance, in case of slender sections. The yield as well as the plastic moments of these specimens were quantified and compared for further evaluation of the development in their local buckling resistance. The test moment capacities were quantified as the product of half the test load (reaction at the support) and the lever arm (shear span). The plastic moment capacities of the specimens were determined by multiplying the measured yield strengths of the specimens with the plastic sectional modulus of the un-reduced cross-section of the built-up beams. From Table 5, we can see that the test yield moment strength of the specimens improved with the incorporation of different novel stiffeners, which is evident by the higher values of M_{Test}/M_y in the stiffened specimens over the control specimens, which further confirms the enhancement in their local buckling strength. It was noted that this improvement was highest (where it crossed the yield moment capacity) in the cross-diagonally stiffened specimens, both for open as well as closed sections.

However, in none of the stiffened specimens did the test moment capacity exceed their plastic moment capacity, primarily due to local buckling failure, *which although was experienced lately, but was a part of the specimen failure, (as observed in Table 5).* The design strength predictions of both NAS (AISI S-100-2016) and IS (IS 801-2010) are highly conservative, except for the reference specimens (Control specimens).

5. Discussions

Apart from local buckling in the compression flange and web, lateral torsional buckling and lateral buckling along the minor axis were the modes of failures observed in specimens with open built-up sections. On the other side, local buckling in the compression flange and web were the prominent modes of failure observed in specimens with closed built-up sections. The box profile of the closed built-up sections was successful in eliminating torsional buckling modes of failure. Hence, serving the intended purpose. Among the reference specimens, the closed built-up section's flexural capacity was higher than the open built-up section. Longitudinal stiffening arrangement as well as cross-diagonal stiffening arrangement improved the flexural performance of both open and closed built-up sections substantially. The cross-diagonal stiffening arrangement was able to enhance the flexural resistance beyond the yield capacity of the section (but not beyond the plastic moment capacity), with its performance being slightly higher in closed built-up sections. However, the performance of longitudinal stiffening arrangement and vertical stiffening arrangement was slightly higher in open built-up sections. Diagonal stiffening arrangement proved to be efficient only in closed built-up sections. The initial stiffness in the all the open and closed built-up sections was nearly same up to a load of about 15 kN and 23 kN respectively, which was mainly because the stiffening action of the novel stiffeners was yet to act. Once their stiffening action responded at higher loading, the stiffness of these novel stiffened specimens was higher than the reference beam specimens. The stiffness of open built-up sections with longitudinal stiffeners was slightly higher than the one with cross diagonal and vertical stiffeners, which was further followed by the one with diagonal end stiffeners. On the contrary, the stiffness of closed built-up sections with cross diagonal stiffeners than the one with longitudinal stiffeners and vertical stiffeners, which was further followed by the one with diagonal end stiffeners. Cross-diagonal stiffening arrangement in both open and closed sections that led to an alternative load path (a sort of truss action) in addition to efficient stiffening may be the reason behind the enhanced flexural resistances in such sections. This arrangement also helped in bringing the specimen's capacity slightly beyond its yield capacity, as shown in Table 5. Also the post failure response was gradual in these sections as compared to others. Inadequate bolting in the bearing stiffeners resulted in its buckling which affected its performance. Fig. 25 shows the efficiency comparison of open and closed series specimens in terms of flexural capacities, stiffness characteristics and strength/weight parameter.

6. Conclusions

This study presented an experimental investigation on the behavior (strength and stiffness characteristics) of built-up open and closed CFS sections beams with various novel stiffening arrangements under four-point loading and simply supported end conditions. The stiffeners were provided in vertical, longitudinal and in diagonal directions in both types of built-up beam sections. The test strengths, stiffness characteristics, failure modes, deformed shapes, load *vs.* mid-span displacements were measured. The test strengths of the beam models are also compared with the design strengths predicted by various standards for CFS structures. Following are the main conclusions drawn:

- Apart from general local buckling in the compression flange and web, lateral torsional buckling and lateral buckling along the minor axis were observed in open built-up sections. However, local buckling in the compression flange and web was prominent in closed built-up sections.
- The flexural capacity of both reference specimens (closed built-up section as well as open built-up section) was nearly the same, with the closed built-up section carrying slightly higher load. However, the box profile of the closed built-up section was successful in eliminating torsional buckling modes of failure. Hence, serving the intended purpose.
- Longitudinal stiffening arrangement as well as cross-diagonal stiffening arrangement improved the flexural performance of both open and closed built-up sections substantially. Hence fulfilling one of the objectives of this study.
- The cross-diagonal stiffening arrangement enhanced the flexural resistance beyond the yield capacity of the section (but not beyond the plastic moment capacity), and performed slightly better in closed built-up sections. However, the opposite was observed on the adoption of longitudinal stiffening and vertical stiffening arrangements. Cross-diagonal stiffening arrangement in both open and closed sections that led to an alternative load path (a sort of truss action) in addition to efficient stiffening may be the reason behind the enhanced flexural resistances in such sections. Furthermore, the post failure response was gradual in these sections as compared to others.
- Buckling of the bearing stiffeners can be avoided by adopting inadequate connections. Hence, it can improve the structural performance of these beams.
- The design strength predictions of both NAS and IS are highly conservative, except for the reference specimens.

The authors are currently working on the numerical study which includes numerical validation and an extensive parametric study on these types of built-up beams. The authors are also planning to bring out reliable design equations for these types of configurations.

References

Acharya, S.R., Sivakumaran, K.S. and Young, B. (2013), "Reinforcement schemes for cold-formed steel joists with a large web opening in shear zone—An experimental investigation", *Thin-Wall. Struct.*, **72**, 28-36. https://doi.org/10.1016/j.tws.2013.06.011

AISI S-100-2016 (2016), North American specification for the design of cold-formed steel structural members, *AISI Standard*, Washington, DC, USA.

Azmi, M., Yatim, M.Y.M., Esa, A. and Badaruzzaman, W.H.W. (2017), "Experimental studies on perforated plate girders with inclined stiffeners", *Thin-Wall. Struct.*, **117**, 247-256. https://doi.org/10.1016/j.tws.2017.04.021

Biggs, K.A., Ramseyer, C., Ree, S. and Kang, T.H. (2015), "Experimental testing of cold-formed built-up members in pure compression", *Steel Compos. Struct., Int. J.*, **18**(6), 1331-1351. https://doi.org/10.12989/scs.2015.18.6.1331

Dar, M.A., Yusuf, M., Dar, A.R. and Raju, J. (2015a), "Experimental study on innovative sections for cold formed steel beams", *Steel Compos. Struct., Int. J.*, **19**(6), 1599-1610. https://doi.org/10.12989/scs.2015.19.6.1599

Dar, M.A., Subramanian, N., Dar, A.R. and Raju, J. (2015b), "Experimental investigations on the structural behaviour of a distressed bridge", *Struct. Eng. Mech., Int. J.*, **56**(4), 695-705. https://doi.org/10.12989/sem.2015.56.4.695

Dar, M.A., Subramanian, N., Dar, A.R. and Raju, J. (2017), "Rehabilitation of a distressed steel roof truss – A study", *Struct. Eng. Mech., Int. J.*, **62**(5), 567-576. https://doi.org/10.12989/sem.2017.62.5.567

Dar, M.A., Sahoo, D.R. and Jain, A.K. (2018a), "Battened built-up cold-formed steel columns: strength and deformation behaviour", *Adv. Concrete Struct. Geotech. Eng., Bloomsbury*, 185-189. (Ed. S.B. Singh, D. Bhunia and G. Muthukumar)

Dar, M.A., Sahoo, D.R., Pulikkal, S. and Jain, A.K. (2018b), "Behaviour of laced built-up cold-formed steel columns: Experimental investigation and numerical validation", *Thin-Wall. Struct.*, **132**, 398-409. https://doi.org/10.1016/j.tws.2018.09.012

Dar, M.A., Subramanian, N., Dar, A.R., Anbarasu, M. and Lim, J.B.P. (2018c), "Structural Performance of Cold-formed Steel Composite Beams", *Steel Compos. Struct., Int. J.*, **27**(5), 545-554. https://doi.org/10.12989/scs.2018.27.5.545

Dar, M.A., Subramanian, N., Dar, A.R., Anbarasu, M., Lim, J.B.P. and Mir, A. (2019a), "Behaviour of partly stiffened cold-formed steel built-up beams : Experimental investigation and numerical validation", *Adv. Struct. Eng.*, **2**(1), 172-186. https://doi.org/10.1177/1369433218782767

Dar, M.A., Sahoo, D.R. and Jain, A.K. (2019b), "Axial compression behavior of laced cold-formed steel built-up columns with unstiffened angle sections", *J. Constr. Steel Res.* **162**. https://doi.org/10.1016/j.jcsr.2019.105727

Fratamico, D.C., Torabiana, S., Zhao, X., Rasmussen, K.J.R. and Schafer, B.W. (2018), "Experimental study on the composite action in sheathed and bare built-up cold-formed steel columns", *Thin-Wall. Struct.*, **127**, 290-305. https://doi.org/10.1016/j.tws.2018.02.002

Haidarali, M.R. and Nethercot, D.A. (2012), "Local and distortional buckling of cold-formed steel beams with both edge and intermediate stiffeners in their compression flanges", *Thin-Wall. Struct.*, **54**, 106-112. https://doi.org/10.1016/j.tws.2012.02.013

Hancock, G.J. (2016), "Cold-formed steel structures: Research review 2013–2014", *Adv. Struct. Eng.*, **19**(3), 1-16. https://doi.org/10.1177/1369433216630145

IS 1608-2005 (2005), Indian Standard- Metallic Materials - Tensile Testing at Ambient Temperature; Bureau of Indian Standards, New Delhi, India.

IS 2062-2011 (2011), Indian Standard, Hot rolled medium and high tensile structural steel specification; Bureau of Indian Standards, New Delhi, India.

IS 801-2010 (2010), Indian Standard- Code of Practice for Use of Cold Formed Light Gauge Steel Structural Members in General Building Construction; Bureau of Indian Standards, New Delhi, India.

Islam, S.M.Z. and Young, B. (2013), "Strengthening of ferritic stainless steel tubular structural members using FRP subjected to Two-Flange-Loading", *Thin-Wall. Struct.*, **62**, 179-190. https://doi.org/10.1016/j.tws.2012.09.001

Islam, S.M.Z. and Young, B. (2014), "FRP strengthening of lean duplex stainless steel hollow sections subjected to web crippling", *Thin-Wall. Struct.*, **85**, 183-200. https://doi.org/10.1016/j.tws.2014.08.010

Keerthan, P. and Mahendran, M. (2013), "Experimental studies of the shear behaviour and strength of lipped channel beams with web openings", *Thin-Wall. Struct.*, **73**, 131-144. https://doi.org/10.1016/j.tws.2013.06.018

Khate, K., Patton, M.L. and Marthong, C. (2018), Structural behaviour of stainless steel stub column under axial compression: a FE study", *Int. J. Steel Struct.*, **18**, 1-18. https://doi.org/10.1007/s13296-018-0083-1

Kim, S., Yom, K. and Choi, S. (2015), "A study on the structural performance of new shape built-up square column under concentric axial load", *Steel Compos. Struct., Int. J.*, **18(**6), 1451-1464. https://doi.org/10.12989/scs.2015.18.6.1451

Kumar, N. and Sahoo, D.R. (2016), "Optimization of lip length and aspect ratio of thin channel sections under minor axes bending", *Thin-Wall. Struct.*, **100**, 158-169. https://doi.org/10.1016/j.tws.2015.12.015

Lawson, R.M., Lim, J., Hicks, S.J. and Simms, W.I. (2006), "Design of composite asymmetric cellular beams and beams with large web openings", *J. Constr. Steel Res.* **62**(6), 614-629. https://doi.org/10.1016/j.jcsr.2005.09.012

Mathison, C., Roy, K., Clifton, G.C., Ahmadi, A., Masood, R. and Lim, J.B.P. (2019a), "Novel pin jointed moment connection for cold-formed steel trusses", *Steel Compos. Struct., Int. J.*, **31**(5), 453-467. https://doi.org/10.12989/scs.2019.31.5.453

Roy, K. Ting, T.C.H., Lau, H.H. and Lim, J.B.P. (2018), "Nonlinear behavior of axially loaded back-to-back built-up cold-formed steel un-lipped channel sections", *Steel Compos. Struct., Int. J.*, **28(**2), 233-250. https://doi.org/10.12989/scs.2018.28.2.233

Roy, K., Lau, H.H. and Lim, J.B.P. (2019), "Finite element modelling of back-to-back built-up cold-formed stainless-steel lipped channels under axial compression", *Steel Compos. Struct., Int. J.*, **33**(1), 869-898. https://doi.org/10.12989/scs.2019.33.1.869

Šakalysa, G. and Daniūnas, A. (2017), "Numerical investigation on web crippling behaviour of cold-formed C-section beam with vertical stiffeners", *Procedia Eng.***,** **172**, 1102-1109. https://doi.org/10.1016/j.proeng.2017.02.171

SP 6-1-2003 (2003), Handbook for Structural Engineers -Part- 1 Structural Steel Sections; Bureau of Indian Standards, New Delhi, India.

SP 6-5-1980 (1980), Handbook for Structural Engineers -Part- 5 Cold-formed, Light-gauge Steel Structures; Bureau of Indian Standards, New Delhi, India.

Subramanian, N. (2016), *Design of Steel Structures-Limit States Method*, (2nd Edition), Oxford University Press, New Delhi, India.

URL, http://www.bundesteel.com

Uzzaman, A., Lim, J.B.P., Nash, D. and Young, B. (2017), "Effects of edge-stiffened circular holes on the web crippling strength of cold-formed steel channel sections under one-flange loading conditions", *Eng. Struct*., **139**, 96-107. https://doi.org/10.1016/j.engstruct.2017.02.042

Valsa Ipe, T., Sharada Bai, H., Manjula Vani, K. and Iqba, M.M.Z. (2013), "Flexural behavior of cold-formed steel concrete composite" *Steel Compos. Struct*., *Int. J*., **14**(2), 105-120. https://doi.org/10.12989/scs.2013.14.2.105

Wang, L. and Young, B. (2014), "Design of cold-formed steel channels with stiffened webs subjected to bending", *Thin-Wall. Struct.*, **85**, 81-92. https://doi.org/10.1016/j.tws.2014.08.002

Wang, L. and Young, B. (2016), "Behavior of Cold-Formed Steel Built-Up Sections with Intermediate Stiffeners under Bending. I: Tests and Numerical Validation", *J. Struct. Eng*., **142**, 1-9. https://doi.org/10.1061/(ASCE)ST.1943-541X.0001428

Wanniarachchi, K.S., Mahendran, M. and Keerthan, P. (2017), "Shear behaviour and design of Lipped Channel Beams with non-circular web openings", *Thin-Wall. Struct.,* **119**, 83-102. https://doi.org/10.1016/j.tws.2017.03.035

Yam, M.C.H., Lam, A.C.C., Wei, F. and Chung, K.F. (2007), "The Local Web Buckling Strength of Stiffened Coped Steel I-Beams", *Steel Struct*.**, 7**, 129-138.

Yam, M.C.H., Ma, M., Lam, A.C.C. and Chung, K.F. (2011), "Experimental study of the strength and behaviour of reinforced coped beams", *J. Constr. Steel Res.*, **67**(11), 1749-1759. https://doi.org/10.1016/j.jcsr.2011.04.015

Yang, Y. and Lui, E.M. (2012), "Behavior and design of steel I-beams with inclined stiffeners", *Steel Compos. Struct., Int. J*., **12**(3), 183-205. https://doi.org/10.12989/scs.2012.12.3.183

Young, B. (2005), "Local buckling and shift of effective centroid of cold-formed steel columns", *Steel Compos. Struct., Int. J.,* **5**(2-3), 235-246. https://doi.org/10.12989/scs.2005.5.2_3.235

DL